The Astrophysical Journal, 818:155 (13pp), 2016 February 20 doi:10.3847/0004-637X/818/2/155

THE ELM SURVEY. VII. ORBITAL PROPERTIES OF LOW-MASS WHITE DWARF BINARIES*

Warren R. Brown[1], A. Gianninas[2], Mukremin Kilic[2], Scott J. Kenyon[1], and Carlos Allende Prieto[3,4]
[1] Smithsonian Astrophysical Observatory, 60 Garden Street, Cambridge, MA 02138 USA; wbrown@cfa.harvard.edu
[2] Homer L. Dodge Department of Physics and Astronomy, University of Oklahoma, 440 W. Brooks Street, Norman, OK, 73019 USA; alexg@nhn.ou.edu, kilic@ou.edu
[3] Instituto de Astrofísica de Canarias, E-38205, La Laguna, Tenerife, Spain; skenyon@cfa.harvard.edu
[4] Departamento de Astrofísica, Universidad de La Laguna, E-38206 La Laguna, Tenerife, Spain; callende@iac.es
Received 2015 November 24; accepted 2016 January 14; published 2016 February 17

ABSTRACT

We present the discovery of 15 extremely low-mass ($5 < \log g < 7$) white dwarf (WD) candidates, 9 of which are in ultra-compact double-degenerate binaries. Our targeted extremely low-mass Survey sample now includes 76 binaries. The sample has a lognormal distribution of orbital periods with a median period of 5.4 hr. The velocity amplitudes imply that the binary companions have a normal distribution of mass with 0.76 $M_\odot$ mean and 0.25 $M_\odot$ dispersion. Thus extremely low-mass WDs are found in binaries with a typical mass ratio of 1:4. Statistically speaking, 95% of the WD binaries have a total mass below the Chandrasekhar mass, and thus are not type Ia supernova progenitors. Yet half of the observed binaries will merge in less than 6 Gyr due to gravitational wave radiation; probable outcomes include single massive WDs and stable mass transfer AM CVn binaries.

Key words: binaries: close – Galaxy: stellar content – white dwarfs

Supporting material: machine-readable tables

1. INTRODUCTION

The extremely low-mass (ELM) Survey is a targeted spectroscopic survey of ELM white dwarfs (WDs). ELM WDs are interesting because the universe is not old enough to form them through single-star evolution. Instead, ELM WDs form out of binary common envelope evolution (Webbink 1984; Iben 1990; Marsh et al. 1995). The result is that ELM WDs are the signposts of ultra-compact double-degenerate binaries, systems that are among the strongest known mHz gravitational wave sources (Brown et al. 2011b; Kilic et al. 2015a).

We use the term ELM WD to describe a WD with surface gravity $5 \lesssim \log g \lesssim 7$ and effective temperature 8000 K $\lesssim T_{\rm eff} \lesssim$ 22,000 K, an empirical definition inspired by the near complete absence of such objects in major spectroscopic WD catalogs (Eisenstein et al. 2006; Gianninas et al. 2011; Kleinman et al. 2013; Kepler et al. 2015). We identify ELM WDs by their spectra: hydrogen Balmer lines provide a sensitive measure of surface gravity in this effective temperature range. ELM WDs are distinct from helium-burning sdB stars that have $T_{\rm eff} > 25{,}000$ K (Heber 2009) at these surface gravities. ELM WDs are also distinct from hydrogen-burning main-sequence stars that have $\log g < 4.75$ at these temperatures (Kepler et al. 2016). Others have referred to similar objects as "low-mass WDs" (Marsh et al. 1995; Moran et al. 1997), "helium-core WD progenitors" (Heber et al. 2003; Silvotti et al. 2012), and "proto-WDs" (Kaplan et al. 2013). Theoretical WD evolutionary models indicate that there can indeed be some ambiguity about the evolutionary status of $\log g \sim 6$ hydrogen atmosphere objects: thermonuclear hydrogen shell flashes, present in $>0.18\,M_\odot$ WD tracks, can cause WDs to loop around in $T_{\rm eff}$–$\log g$ space before they settle on the final cooling track (Sarna et al. 2000; Panei et al. 2007; Althaus et al. 2013; Istrate et al. 2014). Observationally, ELM WDs in eclipsing binaries obey WD mass–radius relations (Steinfadt et al. 2010; Brown et al. 2011b; Parsons et al. 2011; Vennes et al. 2011; Hermes et al. 2014; Kilic et al. 2014b; Hallakoun et al. 2016). Pulsating ELM WDs display pulsation frequencies that validate them as $\simeq 0.2\,M_\odot$ degenerate objects (Hermes et al. 2012c, 2013a, 2013b). We thus feel comfortable calling our $5 < \log g < 7$ objects ELM WDs, whether or not there is residual shell burning. The recent discovery of a pulsating ELM WD in the highly relativistic binary PSR J1738+0333 will enable future, high-precision constraints on the internal structure and evolutionary state of an ELM WD (Kilic et al. 2015b).

Our approach to finding new ELM WDs is to select candidates by broadband color, and then to obtain spectroscopy to identify the nature of the objects. Previous ELM Survey papers have reported the discovery of 73 low-mass WDs, 67 of which are in single-line spectroscopic binaries with orbital periods $P \leqslant 1$ day (Brown et al. 2010, 2012b, 2013; Kilic et al. 2010, 2011a, 2012; Gianninas et al. 2015). The most spectacular object to-date is the $P = 765$ s detached eclipsing WD binary J0651, a gravitational wave source 10,000 times stronger than the Hulse–Taylor pulsar (Brown et al. 2011b; Hermes et al. 2012b).

Here, we present 15 new ELM WD candidates, 9 of which are in short period binaries. We will henceforth refer to any double-degenerate binary that contains an ELM WD as an ELM WD binary. Six of the ELM WD candidates show no significant radial velocity variation. While the non-variable objects have $\log g \simeq 6$, the absence of orbital motion means that we cannot be certain whether or not they are ELM WDs. Kepler et al. (2016) recently identified a population of "sdA" stars at comparable $\log g$ and $T_{\rm eff} \sim 8000$ K in the SDSS spectroscopic catalog. Given that many of our non-variable objects are clumped around 8000 K, and that the number of our non-variable objects is in tension with the number of low inclination binaries expected in a random sample, at least some

* Based on observations obtained at the MMT Observatory, a joint facility of the Smithsonian Institution and the University of Arizona.

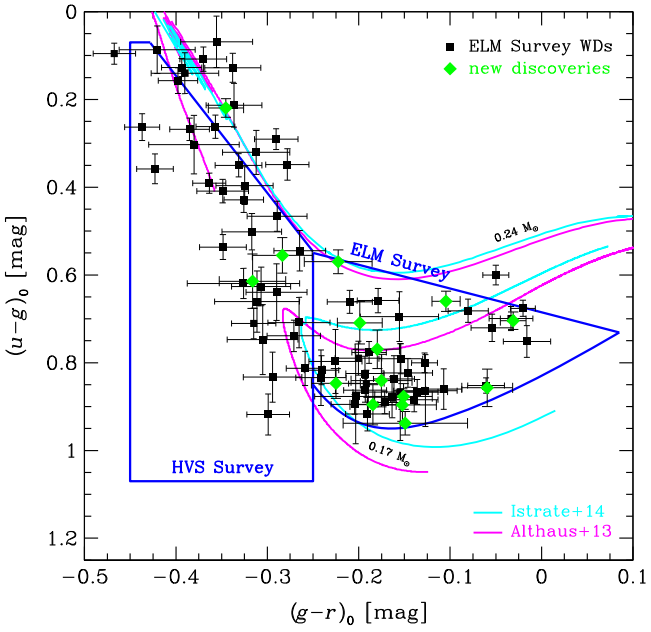

Figure 1. Color–color plot of the ELM Survey. Blue regions indicate our primary target selection regions. New discoveries are marked as green diamonds; previously published WDs are marked as black squares. Cyan and magenta lines show theoretical evolutionary tracks from Istrate et al. (2014) and Althaus et al. (2013), respectively, for 0.17 $M_\odot$ and 0.24 $M_\odot$ models discussed in Section 2.3.

of the non-variable objects may be linked to this sdA stellar population.

We focus our discussion on using the ELM WD binary sample to study the distribution of ELM WD orbital properties. We begin by defining a clean sample of ELM WD binaries for detailed analysis. We fit the observed distribution of orbital period and semi-amplitude, and then derive the distribution of companion mass M_2. The average companion is a 0.76 $M_\odot$ WD, which implies an average binary mass ratio of 1:4 and a total binary mass below the Chandrasekhar mass. The median gravitational merger time of our ELM WD binary sample is 6 Gyr; the likely merger outcomes are stable mass-transfer AM CVn systems and single massive hydrogen-deficient objects, such as extreme helium stars and R CrB stars (Kilic et al. 2010).

2. DATA

We present observations of 15 new ELM WD candidates. Ten objects are selected by color for our targeted spectroscopic ELM Survey program as described in Brown et al. (2012b). Five objects come from follow-up spectroscopy of the completed Hypervelocity Star survey. Hypervelocity Star survey targets are also selected by color, as described in Brown et al. (2012a, 2013).

Figure 1 is a color–color plot showing ELM Survey objects in relation to our approximate target selection regions. We unify the photometry for this paper using de-reddened, point-spread function magnitudes from the Sloan Digital Sky Survey Data Release 12 (SDSS, Alam et al. 2015). We take reddening values from SDSS, and indicate de-reddened photometry and colors with a subscript 0. Objects fall outside our target selection regions for two reasons. First, a handful of ELM WD candidates were selected from the SDSS spectroscopic catalog and thus were not drawn from the HVS Survey and ELM Survey target selection regions (Kilic et al. 2011a, 2012). Second, SDSS photometry has changed since our original target selection: of the five objects published here that come from the HVS Survey, three are now 1–2σ outliers from the HVS Survey target selection region (see green diamonds in Figure 1) presumably due to photometric recalibrations. The SDSS colors for our objects thus have systematic errors comparable to their published statistical errors.

2.1. Spectroscopic Observations

We acquire spectra for the 15 ELM WD candidates using the Blue Channel spectrograph (Schmidt et al. 1989) on the 6.5 m MMT telescope. We configured the Blue Channel spectrograph to obtain 3650–4500 Å spectral coverage with 1.0 Å spectral resolution. We acquire additional spectra for 5 objects using the KOSMOS spectrograph (Martini et al. 2014) on the Kitt Peak National Observatory 4 m Mayall telescope on program numbers 2014B-0119 and 2015A-0082. We configured the KOSMOS spectrograph to obtain 3500–6200 Å spectral coverage with 2.0 Å spectral resolution. We also acquire spectra for objects with $g < 17$ mag using the FAST spectrograph (Fabricant et al. 1998) on the Fred Lawrence Whipple Observatory 1.5 m Tillinghast telescope. We configured the FAST spectrograph to obtain 3500–5500 Å spectral coverage with 1.7 Å spectral resolution.

All spectra were paired with comparison lamp exposures for accurate wavelength calibration. Flux calibration is performed with observations of blue spectrophotometric standards (Massey et al. 1988). We measure radial velocities using the RVSAO cross-correlation program (Kurtz & Mink 1998) with high signal-to-noise templates. Exposure times were chosen to yield a signal-to-noise ratio of 10–15 per resolution element, resulting in typical radial velocity errors of 10–15 km s^{-1} for these WDs.

Our observing strategy is to acquire a single spectrum per target, identify candidate ELM WDs from the initial spectra, then re-observe candidate ELM WDs in subsequent observing runs. If a candidate showed velocity variability, we continue to observe the object until we constrain its orbital solution. If a candidate shows no velocity variability but is confirmed to have $5 < \log g < 7$, we continue to observe it until we can rule out all $P < 1$ day period aliases at high confidence. As a result, each object has around two dozen irregularly spaced observations obtained over a baseline of a few years. The spectra published here were mostly acquired between 2013 January and 2015 October. Figure 2 presents the Balmer line profiles from the summed, rest-frame spectra for our 15 objects. The individual radial velocities are provided in a data table presented in the Appendix.

2.2. Stellar Atmosphere Parameters

We derive the stellar atmosphere parameters for each WD by fitting the summed, rest-frame spectra to a grid of pure hydrogen atmosphere models as described in Gianninas et al. (2011, 2014, 2015). In brief, the models cover 4000 K $< T_{\rm eff} <$ 35,000 K and $4.5 < \log g < 9.5$ and include the Stark broadening profiles from Tremblay & Bergeron (2009). We also apply the Tremblay et al. (2013, 2015) three-dimensional stellar atmosphere model corrections to fix the so-called "log g problem." These corrections can lower the one-dimensional stellar atmosphere model parameters by up to

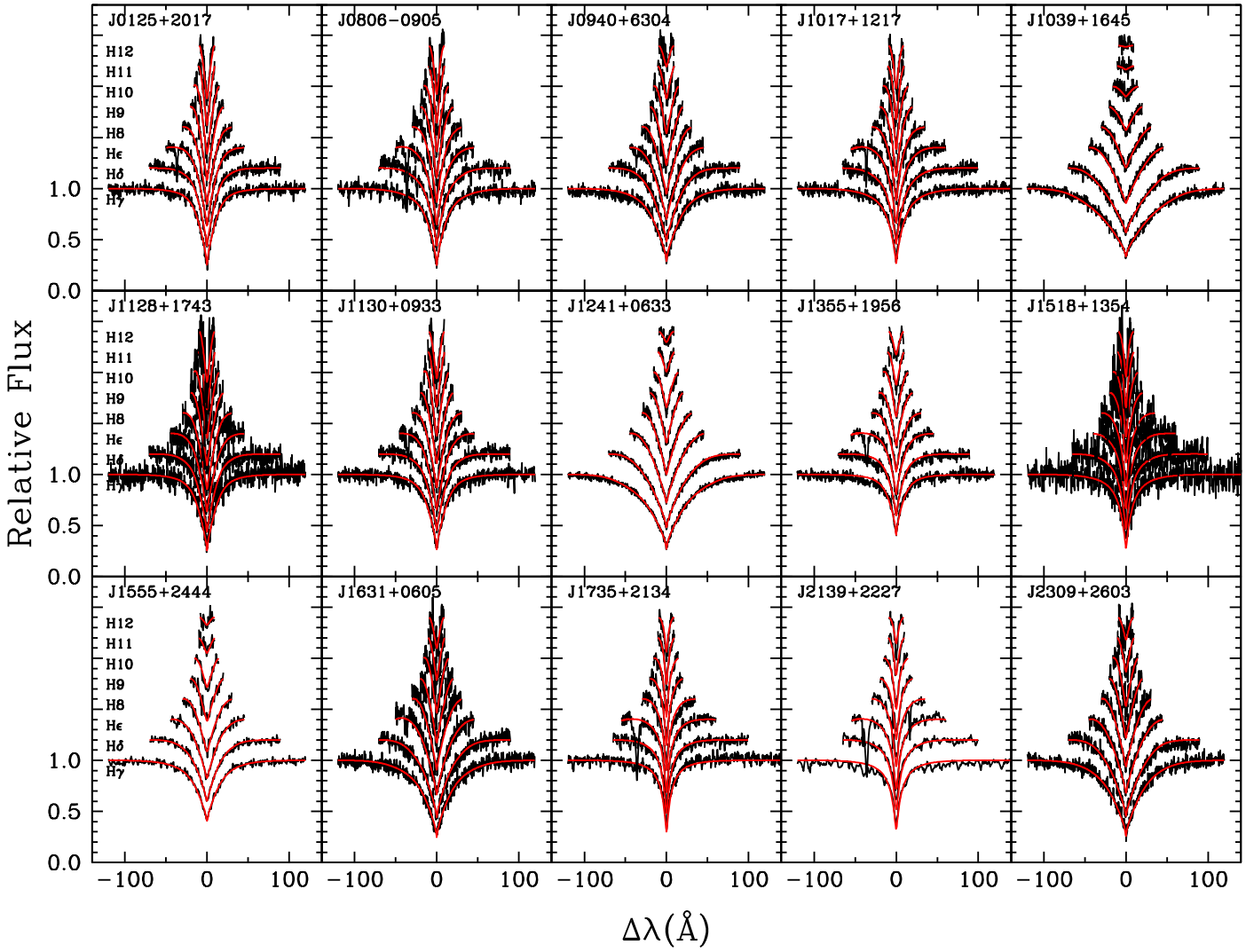

Figure 2. Model fits (smooth red lines) overplotted on the composite observed spectra (black lines) for the 15 new low-mass WDs.

Table 1
WD Physical Parameters

Object	R.A. (h:m:s)	decl. (d:m:s)	$T_{\rm eff}$ (K)	$\log g$ (cm s^{-2})	Mass ($M_\odot$)	g_0 (mag)	M_g (mag)	$d_{\rm helio}$ (kpc)
J0125+2017	1:25:16.758	20:17:44.63	11170 ± 200	4.709 ± 0.062	0.184 ± 0.010	17.153 ± 0.021	4.88 ± 0.18	2.855 ± 0.238
J0806−0905	8:06:53.308	−9:05:11.51	8510 ± 130	5.116 ± 0.104	0.166 ± 0.011	17.681 ± 0.006	6.88 ± 0.22	1.454 ± 0.145
J0940+6304	9:40:08.729	63:04:27.40	12910 ± 210	5.964 ± 0.050	0.180 ± 0.010	19.618 ± 0.026	7.69 ± 0.13	2.436 ± 0.150
J1017+1217	10:17:07.109	12:17:57.42	8330 ± 130	5.528 ± 0.062	0.142 ± 0.012	17.479 ± 0.020	8.13 ± 0.23	0.745 ± 0.083
J1039+1645	10:39:53.118	16:45:24.28	14310 ± 240	7.639 ± 0.046	0.458 ± 0.018	18.941 ± 0.024	10.71 ± 0.08	0.444 ± 0.018
J1128+1743	11:28:23.334	17:43:54.58	11260 ± 210	4.756 ± 0.063	0.183 ± 0.010	19.434 ± 0.026	4.99 ± 0.18	7.774 ± 0.656
J1130+0933	11:30:27.956	9:33:03.55	12020 ± 210	5.062 ± 0.057	0.179 ± 0.010	16.843 ± 0.029	5.62 ± 0.16	1.761 ± 0.133
J1241+0633	12:41:24.291	6:33:51.02	11280 ± 170	6.648 ± 0.047	0.199 ± 0.012	17.722 ± 0.021	9.64 ± 0.09	0.413 ± 0.018
J1355+1956	13:55:12.336	19:56:45.43	8050 ± 120	6.101 ± 0.064	0.156 ± 0.010	16.098 ± 0.024	9.76 ± 0.17	0.185 ± 0.014
J1518+1354	15:18:02.566	13:54:31.96	8080 ± 120	5.435 ± 0.071	0.147 ± 0.018	18.988 ± 0.019	8.00 ± 0.34	1.594 ± 0.246
J1555+2444	15:55:02.000	24:44:22.05	18170 ± 310	6.296 ± 0.051	0.190 ± 0.012	16.045 ± 0.015	7.82 ± 0.12	0.443 ± 0.025
J1631+0605	16:31:23.675	6:05:33.82	10150 ± 170	5.818 ± 0.069	0.162 ± 0.010	19.002 ± 0.019	8.08 ± 0.17	1.533 ± 0.118
J1735+2134	17:35:21.694	21:34:40.64	7940 ± 130	5.758 ± 0.081	0.142 ± 0.010	15.904 ± 0.011	9.06 ± 0.21	0.235 ± 0.023
J2139+2227	21:39:07.415	22:27:08.87	7990 ± 130	5.932 ± 0.121	0.149 ± 0.011	15.600 ± 0.011	9.42 ± 0.29	0.174 ± 0.023
J2309+2603	23:09:19.904	26:03:46.69	10950 ± 160	6.127 ± 0.057	0.176 ± 0.010	18.986 ± 0.016	8.54 ± 0.14	1.229 ± 0.080

Note. $T_{\rm eff}$ and $\log g$ values are corrected for 3D effects following Tremblay et al. (2015). Mass and M_g values are estimated with Althaus et al. (2013) models.

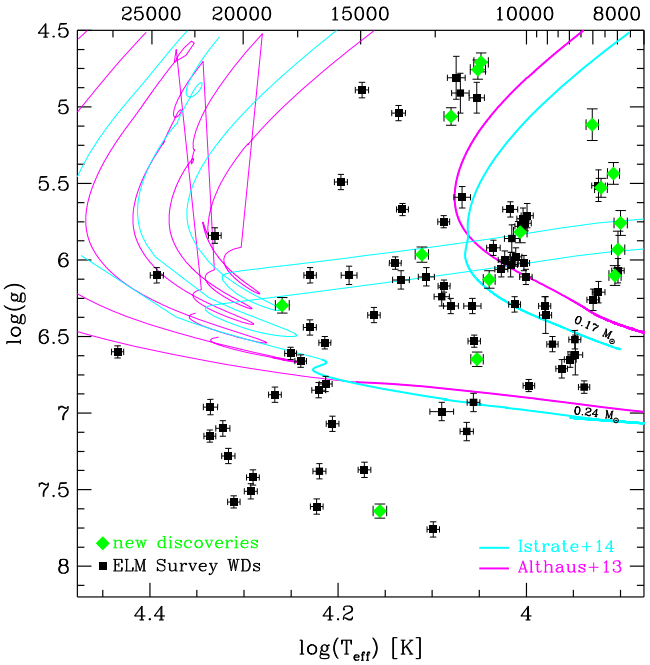

Figure 3. Surface gravity vs. effective temperature plot for the ELM Survey. New discoveries are marked as green diamonds; previously published WDs are marked as black sqaures. Cyan and magenta lines show evolutionary tracks from Istrate et al. (2014) and Althaus et al. (2013), respectively, for 0.17 $M_{\odot}$ and 0.24 $M_{\odot}$ models. Short-lived parts of the tracks are indicated by thin lines (upper left corner); long-lived parts of the tracks are indicated by thick lines (right side). Our color selection effectively samples $8000 < T_{\rm eff} < 22{,}000$ K.

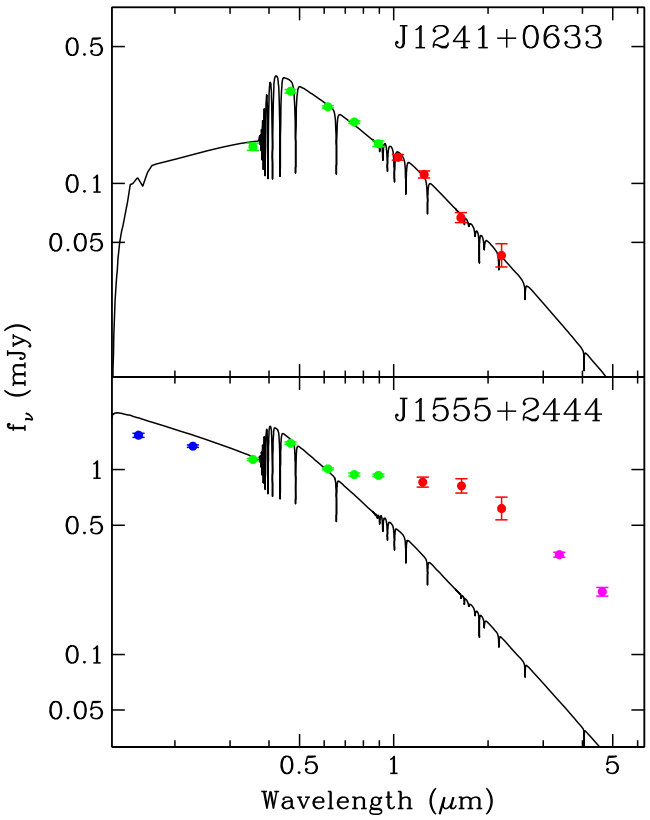

Figure 4. Comparison of the spectroscopic stellar atmosphere model (black line) to available photometry from *GALEX* (blue points), SDSS (green points), 2MASS or UKIDSS (red points), and *WISE* (magenta points). J1241+0633 is a typical example, while J1555+2444 is a notable exception: a WD + M dwarf.

500 K in $T_{\rm eff}$ and 0.3 dex in $\log g$. Our statistical uncertainties are typically $\pm$180 K in $T_{\rm eff}$ and $\pm$0.07 dex in $\log g$.

The best-fit models are over-plotted on each spectrum in Figure 2. We mask the region around the Ca II K line when doing the Balmer line fits. Twelve of our new WDs have $5 < \log g < 7$ and are thus ELM WDs. Two objects, J0125+2017 and J1128+1743, have anomalously low surface gravities $\log g \simeq 4.7$ consistent with metal-poor, young, main-sequence stars, however, they both show short-period orbital motion and are probable ELM WDs (see Section 3.2). The last object, J1039+1645, is a slightly more massive $\log g = 7.64$ WD that also shows orbital motion. Table 1 presents the stellar atmosphere parameters for all 15 objects.

Figure 3 plots the distribution of $T_{\rm eff}$ and $\log g$ for the ELM Survey objects. Our $(g-r)_0$ target selection results in an approximate temperature selection of $8000{\rm K} < T_{\rm eff} < 22{,}000$ K. The observed range of surface gravity reflects our choice to follow-up those objects with initial surface gravity estimates $5 \lesssim \log g \lesssim 7$. The clump of new objects around 8000 K is from the non-variable objects.

We validate our stellar atmosphere parameters by comparing the best spectroscopic model for each object against photometry from *GALEX* (Martin et al. 2005), SDSS (Alam et al. 2015), 2MASS (Skrutskie et al. 2006), UKIDSS (Lawrence et al. 2007), and *WISE* (Wright et al. 2010). We do not derive parameters from the spectral energy distributions because many of the fainter ELM WDs lack ultraviolet and infrared photometry. Instead, we compare available photometry to the best spectroscopic fit as a consistency check. We generally find excellent agreement between the models and the observed spectral energy distributions. J1241+0633, for example, has a reduced χ^2 of 1.15 (see Figure 4). A notable exception is J1555+2444, the first WD + M dwarf in the ELM Survey, which has a reduced χ^2 of 181. WD + M dwarf binaries are common (e.g., Rebassa-Mansergas et al. 2012), however our *ugri* color selection is designed to exclude such systems. In the case of J1555+2444, the M dwarf contributes significant flux in the near-infrared bands (see Figure 4). We discuss this system further below.

2.3. WD Parameters

We estimate WD mass and luminosity using the recent ELM WD evolutionary tracks of Althaus et al. (2013) and of Istrate et al. (2014). Both sets of tracks adopt neutron star companions for their evolutionary calculations, but an ELM WD's evolution should be unaffected by its companion once it detaches from the common envelope. The choice of progenitor metallicity, on the other hand, can have a significant impact on the hydrogen envelope mass and resulting cooling times (Althaus et al. 2015). Both sets of ELM WD tracks assume solar metallicity appropriate for disk objects; our ELM Survey sample contains both disk and halo objects.

For reference, we plot fiducial 0.17 $M_{\odot}$ and 0.24 $M_{\odot}$ ELM WD tracks in Figures 1 and 3. We draw Althaus et al. (2013) tracks in magenta and Istrate et al. (2014) tracks in cyan. In Figure 1, we plot estimated synthetic colors to compare with our color selection. In Figure 3, we plot the published tracks, and use thin lines to indicate the short-lived parts of the tracks and thick lines to indicate the long-lived parts of the tracks. Shell flashes, which generate loops and lead to faster evolution,

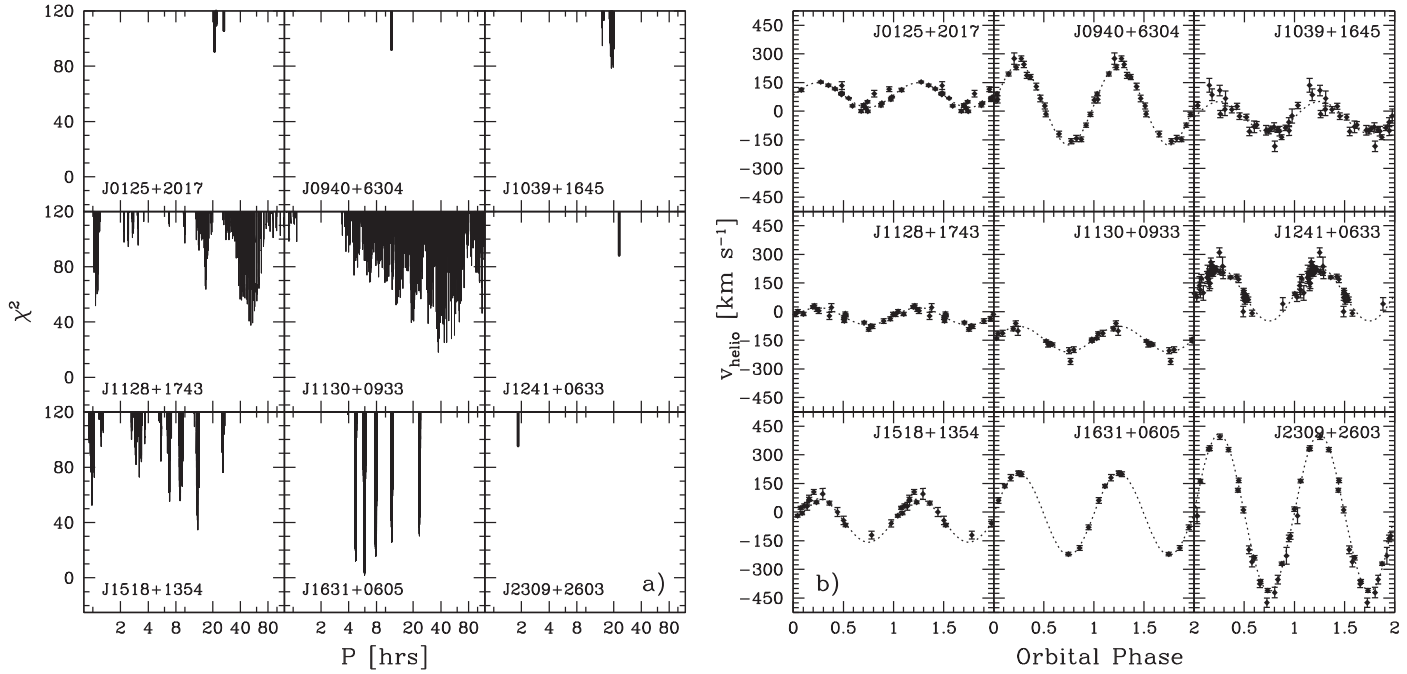

Figure 5. (a) Periodograms for the 9 WDs with significant orbital motion. The best orbital periods have the smallest χ^2. Period aliases, with the exception of $P \simeq 2$ day aliases in J1130+0933, are at least $\Delta\chi^2 =$ 15–20 larger than the minima and are likely insignificant. (b) Observed velocities phased to the best-fit orbits.

are present in the $0.24\,M_\odot$ tracks and absent in the $0.17\,M_\odot$ tracks.

We interpolate the evolutionary tracks to determine the mass and luminosity for each of our objects, however the interpolation is complicated by the fact that the tracks map phase space in a discrete and irregular way. Our solution is to identify the two nearest tracks to an observed $T_{\rm eff}$ and $\log g$ value, and interpolate between those two tracks on the basis of $\log g$. We then Monte Carlo our $T_{\rm eff}$ and $\log g$ with their uncertainties to derive the mass and luminosity uncertainties.

The evolutionary tracks of Althaus et al. (2013) and Istrate et al. (2014) yield very similar mass and luminosity estimates for our objects. Consider the ELM Survey WDs in the mass range over which the two sets of tracks overlap: $0.16 < M < 0.30\,M_\odot$. For these 66 objects, the two sets of tracks differ on average by $0.007\,M_\odot$ (systematic) $\pm 0.012\,M_\odot$ (statistical) in mass and 0.044 mag (systematic) ± 0.068 mag (statistical) in absolute g-band magnitude M_g. Istrate et al. (2014) tracks yield slightly more massive and more luminous estimates, likely due to the lack of gravitational settling in the models resulting in mixed H/He atmospheres. In any case, Althaus et al. (2013) tracks span a wider range of mass and so are more convenient to use with the entire ELM Survey sample. We adopt Althaus et al. (2013) tracks for the following discussion, and add $0.01\,M_\odot$ in quadrature to the formal mass uncertainty to account for the uncertainty in the choice of model. Table 1 presents the parameters, including the dereddened apparent g-band magnitudes and distances, for all 15 WDs.

2.4. Orbital Elements

Before determining orbital elements, we must first separate the radial velocity variable and non-variable objects. We use the F-test to quantify how the variance of the radial velocities around a constant mean velocity compares to the variance around a best-fit orbital solution (e.g., Bevington & Robinson 1992). The larger the F-test probability, the more likely the orbital solution is consistent with noise. Six of the ELM WDs published here are significantly non-variable, with F-test probabilities >0.01 and typical 95% confidence upper-limits on semi-amplitude of $k < 30\,{\rm km\,s^{-1}}$. We discuss the non-variable ELM WDs further below.

Nine WDs have significant velocity variability, with F-test probabilities <0.002. We calculate orbital elements for these nine WDs in the same way as in prior ELM Survey papers. In brief, we use the summed spectra as cross-correlation templates to maximize the velocity precision for each individual object, and then minimize χ^2 for a circular orbit using the code of Kenyon & Garcia (1986). We search for orbital periods up to 5 days, which is the maximum time span of our individual observing runs and a period at which a $0.6\,M_\odot$ WD companion (assuming $i = 60°$) produces a detectable $k = 75\,{\rm km\,s^{-1}}$. Figure 5 shows periodograms and phased radial velocity plots for the nine WDs. We estimate the significance of the period aliases using χ^2 values. For normally distributed errors, a $\Delta\chi^2 = 13.3$ with respect to the minimum value corresponds to a 99% confidence interval for 4 degrees of freedom (Press et al. 1992). On this basis, J1130+0933 has significant period aliases around 2 days, but we consider these aliases uninteresting given that they are longer than the best 1.6 day period. For all other objects, the period aliases have $\Delta\chi^2 =$ 15–20 larger than the minimum and thus appear insignificant. Table 2 presents the orbital elements. The full ELM Survey sample of 88 objects is provided in a data table presented in the Appendix.

2.5. ELM Survey Completeness

Over the magnitude range $15 < g_0 < 20$, we have obtained spectra for 99% of the stars in the HVS Survey target selection region (Brown et al. 2012b) and 80% of the stars in the ELM

Table 2
Binary Orbital Parameters

Object	N_{obs}	P (days)	k (km s^{-1})	γ (km s^{-1})	M_2 ($M_\odot$)	τ (Gyr)
J0125+2017	16	0.88758 ± 0.00004	65.4 ± 2.1	79.4 ± 2.2	>0.14	<938.3
J0806−0905	16	…	<28.5	109.4 ± 3.7	…	…
J0940+6304	20	0.48438 ± 0.00001	210.4 ± 3.2	32.6 ± 2.3	>0.73	<51.27
J1017+1217	14	…	<30.2	24.8 ± 3.6	…	…
J1039+1645	26	0.82470 ± 0.02214	83.4 ± 4.0	−32.9 ± 2.8	>0.31	<186.2
J1128+1743	21	2.16489 ± 0.03889	41.2 ± 2.0	−24.5 ± 1.4	>0.11	<12350
J1130+0933	16	1.55935 ± 0.00014	69.0 ± 3.9	−145.6 ± 1.8	>0.19	<3241
J1241+0633	40	0.95912 ± 0.00028	138.2 ± 4.8	90.0 ± 3.3	>0.51	<377.6
J1355+1956	33	…	<40.9	−41.8 ± 3.9	…	…
J1518+1354	16	0.57655 ± 0.00734	112.7 ± 4.6	−43.4 ± 3.0	>0.23	<237.6
J1555+2444	20	…	<23.0	1.0 ± 3.2	…	…
J1631+0605	9	0.24776 ± 0.00411	215.4 ± 3.4	−9.6 ± 3.7	>0.47	<13.15
J1735+2134	20	…	<31.6	−16.3 ± 3.4	…	…
J2139+2227	37	…	<22.0	8.5 ± 2.7	…	…
J2309+2603	15	0.07653 ± 0.00001	405.8 ± 3.5	−14.8 ± 2.6	>0.79	<0.359

Survey target selection region (Figure 1). In absolute numbers, 120 of 589 ELM Survey targets remain unobserved. Almost all of the 120 unobserved targets are located between R.A. = 21 hr and R.A. = 3 hr due to telescope time allocation and weather. Based on current detection rates, we estimate that 26% of the remaining targets are likely DA WDs, of which one third (or about 10) are likely ELM WD binaries.

Our multi-epoch follow-up spectroscopy is less complete. We currently have 26 ELM WD candidates that require confirming observations, and another 17 velocity variable ELM WDs that have poorly constrained orbital parameters. Summing these numbers together with the unobserved targets suggests there may be another ≃53 ELM WD binaries in our target selection regions. Our published sample currently contains 76 binaries. We therefore estimate that the published ELM Survey sample is approximately 60% complete for ELM WD binaries.

3. RESULTS

We discuss the 15 new ELM WD candidates in this section, starting with the 1.8 hr orbital period binary system J2309+2603. The other eight double degenerate binaries fill out the longer orbital period portion of our sample. Our understanding of these systems is based on multi-epoch spectroscopy and broadband colors; we do not yet have time-series photometry for these systems. We investigate the possible ELM WD + M dwarf system J1555+2444, and discuss the statistics of the non-velocity variable ELM WD candidates.

3.1. J2309+2603

SDSS J230919.904+260346.69 (hereafter J2309+2603) is a 0.176 $M_\odot$ ELM WD with a 1.8367 ± 0.0002 hr orbital period and a 412.4 ± 2.7 km s^{-1} semi-amplitude. Given Kepler's 3rd Law, the minimum mass companion to this ELM WD is a 0.82 $M_\odot$ object at an orbital separation of 0.76 $R_\odot$. If we adopt the mean inclination angle for a random stellar sample, $i = 60°$, the companion is a 1.14 $M_\odot$ object at an orbital separation of 0.83 $R_\odot$. There is no evidence for mass-transfer in this system. Thus the ELM WD's most likely companion is another WD.

There remains a 20% likelihood, assuming a random distribution of inclinations, that the companion is a $1.4 < M_2 < 3.0\,M_\odot$ neutron star. Given that this putative neutron star would have accreted material during the common envelope evolution of the ELM WD progenitor, J2309+2603 is possibly a millisecond pulsar binary system. However no gamma-ray source exists at this position in the *Fermi* Large Area Telescope source catalog (Acero et al. 2015). A targeted *Chandra* search of other high-probability candidates in the ELM Survey has also found no neutron star companions (Kilic et al. 2014b). We conclude that J2309+2603 is most likely a double WD binary with a total binary mass near the Chandrasekhar mass.

J2309+2603 is losing energy and angular momentum to gravitational wave radiation. The timescale for the binary to shrink and begin mass transfer via Roche-lobe overflow is given by the gravitational wave merger time

$$\tau = 47925 \frac{(M_1 + M_2)^{1/3}}{M_1 M_2} P^{8/3}\ \mathrm{Myr}, \quad (1)$$

where the masses are in $M_\odot$ and the period P is in days (Kraft et al. 1962). The merger time is 350 Myr for the minimum mass companion, and shorter if the companion is more massive.

3.2. Eight Other Double Degenerate Binaries

The other eight double degenerate binaries are longer orbital period, lower semi-amplitude systems (see Figure 5). The radial velocity constraints vary by object, and there is little to say about the best-measured system. J0940+6304 has complete phase coverage and excellent constraints on period and semi-amplitude.

J1241+0633 and J1518+1354 have excellent phase coverage and orbital period constraints, but increased semi-amplitude uncertainties due to a relative lack of observations near velocity minimum. J1631+0605 is a P = 5.946 ± 0.099 hr binary with a well-constrained period and semi-amplitude—observations were obtained at quadrature on back-to-back nights—however incomplete phase coverage allows for the possibility of a modestly ($e \leqslant 0.3$) eccentric orbit. Given that none of the other 75 binaries in the ELM Survey have significant eccentricity, nor do we expect much eccentricity from the common envelope origin of the ELM WD, we adopt the circular orbit solution. J1039+1645, J1128+1743, and J1130+0933, by comparison, have excellent phase coverage but exhibit period aliases clumped around

their best-fit periods. Given that the observations rule out significantly different orbital periods for each object, we consider the 3% uncertainty in period acceptable. Systems with $P > 16$ hr orbital periods have >100 Gyr merger times. The median likelihood for a neutron star companion in each of the eight longer-period binaries is 4%.

We note that J0125+2017 and J1128+1743 are abnormally low surface gravity objects, with $\log g \simeq 4.7$, $T_{\rm eff} \simeq 11{,}200$ K, and masses around $0.19\,M_{\odot}$ if they are ELM WDs. Their low $k \simeq 50$ km s^{-1} semi-amplitudes imply that the unseen companions are comparable $0.2\,M_{\odot}$ mass objects at $2.5\,R_{\odot}$ orbital separations (assuming $i = 60°$). Alternatively, it is possible these objects are very metal-poor, young, main-sequence stars. Padova tracks show that a $1.6\,M_{\odot}$, $Z = 0.0001$ star has similar $T_{\rm eff}$ and $\log g$ at <100 Myr ages (Bressan et al. 2012). If J0125+2017 and J1128+1743 are very metal-poor, main-sequence stars, their orbital motion would be due to $0.4\,M_{\odot}$ mass companions at $4.5\,R_{\odot}$ orbital separations. Very metal-poor, main-sequence stars should not be forming near the Sun, but blue stragglers are possible (e.g., Brown et al. 2008). However, observed blue stragglers have typical orbital periods of ~1000 days (Geller & Mathieu 2012; Geller et al. 2015). Because J0125+2017 and J1128+1743 have orbital periods of 21 hr and 52 hr, respectively, we believe they are most likely ELM WD binaries.

3.3. J1555+2444

J1555+2444 is a possible ELM WD + M dwarf system. The M dwarf is classified as an $0.43\,M_{\odot}$ M2 star (Rebassa-Mansergas et al. 2010; Schreiber et al. 2010). Assuming that the M2 star dominates the z-band flux and has absolute magnitude $M_z = +8.0$ (Bressan et al. 2012), its distance is about 0.51 kpc. This is consistent with the 0.44 kpc and 0.49 kpc distance estimates to the hot $T_{\rm eff} = 18{,}170$ K ELM WD using Althaus et al. (2013) and Istrate et al. (2014) tracks, respectively. Thus J1555+2444 could be a legitimate WD + M dwarf system.

The ELM WD shows no orbital motion, however. We constrain its orbital semi-amplitude to have a 95% confidence upper limit of $k < 23$ km s^{-1} on the basis of 6 epochs of radial velocities obtained over 2 years. This result is in tension with the work of Nebot Gómez-Morán et al. (2011), who find that the period distribution of WD + main-sequence binaries peaks around $P = 10.3$ hr. The orbital period of J1555+2444 would have to be 3 months, assuming $i = 60°$, to be consistent with the observed semi-amplitude limit. Alternatively, the orbital inclination would have to be $i < 8°$, assuming $P = 10.3$ hr, to be consistent with the observed semi-amplitude limit, an inclination that has a 1% likelihood in a random distribution.

An ELM WD + M dwarf binary is also unlikely from a stellar evolutionary standpoint. The standard ELM WD formation scenario requires double common-envelope evolution in which the companion star evolves first. Other possibilities are that this is a triple system in which the M dwarf is an outer third, or else a chance super-position of an M dwarf and ELM WD. J1555+2444 thus shares some similarities to J0935+4411, the 20 minutes orbital period double WD binary that appears to have an M dwarf along the line of sight (Kilic et al. 2014a). Additional observational constraints are needed to understand the nature of this object.

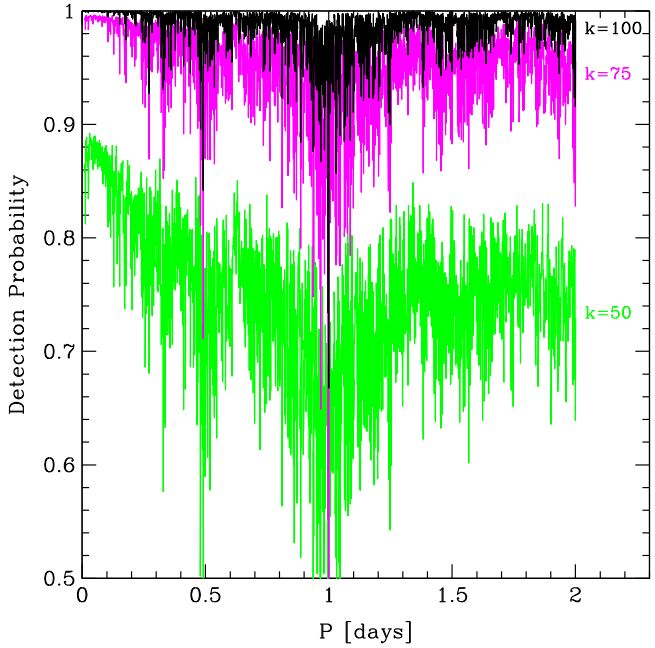

Figure 6. Likelihood of detecting $k = 50$ (green), 75 (magenta), and 100 (black) km s^{-1} orbital motion as a function of period P given our set of observations for the six non-variable ELM WDs.

3.4. Non-variable Objects: ELM WDs or sdA Stars

Given that ELM WDs are the likely end product of compact binary evolution, the discovery of J1555+2444 and the five other non-variable objects is surprising. An obvious question is whether our observations have missed potential companions. We explore the sensitivity of our radial velocities to different possible orbital periods and semi-amplitudes following the procedure described by Brown et al. (2013): we Monte-Carlo the observed velocities with their errors, and count the number of 10,000 orbital fits that have F-test probabilities <0.01 for orbital periods between 0.1 and 2 days.

Figure 6 presents the averaged result for the six non-variable ELM WD candidates. The lines in Figure 6 represent the probability of detecting $k = 50$, 75, and 100 km s^{-1} orbits as a function of P given our set of observations. The objects have 6 or 7 epochs of time-series spectroscopy and a total of a couple dozen observations each. Figure 6 shows that while our ground-based observations are naturally less sensitive around 12 and 24 hr orbital periods, we are sensitive to almost any orbit with $k > 75$ km s^{-1}. On average, our observations should detect 95% of binary systems with $k = 75$ km s^{-1} and 99% of binary systems with $k = 100$ km s^{-1} out to $P = 2$ day orbital periods. Yet our observations show that the non-variable systems have a typical 95% confidence upper limit of $k < 30$ km s^{-1}.

While we expect to find some binaries in face-on orientations, it is hard to explain all of the non-variable ELM WD candidates in this way. Restricting ourselves to the 78 best ELM WD candidates in our Survey, those objects with $\log g < 7.15$, we find 67 binaries and 11 non-variable objects. The median semi-amplitude of the ELM WD binaries is $k = 220$ km s^{-1}, a semi-amplitude that would appear <75 km s^{-1} for $i < 20°$ inclinations. Assuming a random distribution of inclinations, only 5 of the 78 objects with $\log g < 7.15$ should have $i < 20°$. Yet 11 of the 78 objects are

non-variable. If we adopt the uncertainty as $\sqrt{N}$, the excess of non-variable objects appears significant at the 2.5-σ level. This excess suggests that the non-variable ELM WD candidates in our sample may not all be face-on binary systems.

To avoid possible bias in relying on observed semi-amplitudes, we can instead assume a companion mass distribution M_2 and ask what fraction of binaries should fall below our detection threshold. If we adopt the lognormal orbital period distribution (allowing $0 < P < \infty$) and the normal M_2 distribution derived below (Section 4) and assume a random distribution of inclinations, 6.5 of 78 binaries should have $k < 75$ km s^{-1}. This number is in 2-σ disagreement with the number of observed non-variable ELM WD candidates. While not formally significant, it is suggestive that Maxted et al. (2000) find a similar excess of non-variable objects in their sample of $<0.5\,M_\odot$ low-mass WDs. Thus our non-variable objects are possibly binaries with long orbital periods, or they are possibly something else altogether.

Notably, 8 of the 11 non-variable ELM WD candidates are found clumped together around $T_{\rm eff} \simeq$ 8000 K at the cool edge of our Survey. Kepler et al. (2016) recently identified thousands of similar "sdA" stars with $T_{\rm eff} \sim 8000$ K and $\log g \sim 6$ in the SDSS spectroscopic catalog. The non-variable ELM candidates are possibly linked to these sdA stars, however the sdA stars cannot be ELM WDs on the basis of their numbers. According to the evolutionary tracks, an ELM WD spends about as much time with $7500 < T_{\rm eff} < 8500$ K as it spends at $8500\ {\rm K} < T_{\rm eff} < 22{,}000$ K. Shell flashes can cause the time spent in these temperature ranges to differ by a factor of 2, but not by a factor of 10. The models also show that 8000 K ELM WDs are about 3 mag fainter in M_g than 12,000 K ELM WDs. Taken together, a magnitude-limited survey should observe fewer ELM WDs at 8000 K than at higher temperatures. Yet the sdA stars of Kepler et al. (2016) are over 10 times more abundant than our higher-$T_{\rm eff}$ ELM WD binaries in the same footprint of sky. We conclude that the sdA stars are probably unrelated to ELM WDs.

Our 8 non-variable objects with $T_{\rm eff} \simeq$ 8000 K are possibly related to the sdA stars. If true, this would explain why we find so many non-variable objects around 8000 K. The three hotter non-variable objects would then be consistent at the 1σ level with the number of ELM WDs we would expect to find in face-on binaries in our color-selected survey. Given the ambiguity about the nature of the non-variable objects, we focus the remainder of this paper on the ELM WD binaries.

4. ANALYSIS AND DISCUSSION

4.1. Clean Sample

We begin by defining a clean sample of ELM WD binaries, and then use that sample to derive the orbital period and secondary mass distributions of the sample. We construct a clean sample of ELM WD binaries by first taking the 88 published ELM Survey objects and excluding the 12 non-variable objects. We further restrict the sample to those binaries with $k > 75$ km s^{-1}, a semi-amplitude threshold above which our catalog should be 95% complete (Figure 6). The ELM Survey color selection provides a built-in temperature selection, but the $\log g$ selection is more ambiguous. Tremblay et al. (2015) 3D corrections push some of the WD surface gravities below $\log g = 5$. We have also obtained observations for every WD near $\log g \simeq 7$ during the course of our survey. Since we would like to maximize our number statistics, we choose to restrict our sample to $4.85 < \log g < 7.15$, a range over which the ELM Survey observations should be reasonably complete. Taken together, these cuts leave us with a clean sample of 62 ELM WD binaries. We present the clean sample in Table 3 sorted by orbital period.

4.2. Orbital Period Distribution

Next, we consider the orbital period distribution of the clean sample, plotted in Figure 7. The median orbital period of the clean sample is 0.226 days, or 5.4 hr.

We use the non-parametric Anderson–Darling test to evaluate the goodness of fit between a model distribution and the observations (Scholz & Stephens 1987). The p-value of the Anderson–Darling test is the probability that the model and observations share a common distribution. A p-value of zero rejects the null hypothesis that the model and observations share a common distribution.

We fit different functional forms to the period distribution and find that the observations are best matched by a lognormal distribution,

$$f_P\,(P;\,\mu_P,\,\sigma_P^2) \;=\; \frac{1}{P\sqrt{2\pi}\,\sigma_P}\exp\left(-\frac{(\ln P - \mu_P)^2}{2\sigma_P^2}\right), \qquad (2)$$

where P is the period, μ_P is the lognormal mean, and σ_P is the standard deviation. We restrict the fit to $P < 1.1$ day to match the absence of orbital periods greater than $\simeq$1 day in the clean sample. The green lines in Figure 7 show the best fit for lognormal mean $\mu_P = -1.28$ and standard deviation $\sigma_P = 1.34$. The Anderson–Darling p-value is 0.999, indicating a strong consistency between the model and the observations.

4.3. Secondary Mass Distribution

We now derive the (unseen) secondary mass distribution by considering the distribution of observables. Formally, the observed orbital period P, semi-amplitude k, and derived ELM WD mass M_1 are related to the secondary mass M_2 and orbital inclination i by the binary mass function,

$$\frac{Pk^3}{2\pi G} \;=\; \frac{(M_2 \sin i)^3}{(M_1 + M_2)^2}. \qquad (3)$$

Given our surface gravity constraints, the ELM WD mass distribution M_1 is narrow and centered around $\sim 0.2\,M_\odot$. Thus most of the information about M_2 is encoded in the semi-amplitude distribution. Inclinations of individual binaries are unknown, however the target selection is known: the ELM WDs were targeted by color. Thus we will assume that the inclination distribution is random in $\sin i$ above our detection threshold.

Our computational approach is to Monte Carlo different trial distributions of M_2. We draw inclination from a random $\sin i$ distribution and P from the observed lognormal distribution. We clip the simulations to match the observational $k > 75$ km s^{-1} sample limit, a threshold that translates into an $i \gtrsim 20^\circ$ limit in inclination. We then use the Anderson–Darling test to quantify how likely the simulated and observed distributions of semi-amplitude share a common distribution.

Table 3
Clean Sample of ELM WD Binaries

Object	P (days)	k (km s^{-1})	M_1 ($M_\odot$)	M_1/M_2	$M_{\rm tot}$ ($M_\odot$)	τ (Gyr)
0651+2844	0.00886 ± 0.00001	616.9 ± 5.0	0.247 ± 0.015	$0.50^{+0.01}_{-0.01}$	$0.74^{+0.01}_{-0.01}$	$0.001^{+0.0001}_{-0.0001}$
0935+4411	0.01375 ± 0.00051	198.5 ± 3.2	0.313 ± 0.019	$0.42^{+0.20}_{-0.10}$	$1.07^{+0.25}_{-0.24}$	$0.002^{+0.0008}_{-0.0004}$
0106−1000	0.02715 ± 0.00002	395.2 ± 3.6	0.189 ± 0.011	$0.33^{+0.05}_{-0.09}$	$0.75^{+0.21}_{-0.07}$	$0.027^{+0.003}_{-0.006}$
1630+4233	0.02766 ± 0.00004	295.9 ± 4.9	0.298 ± 0.019	$0.39^{+0.17}_{-0.10}$	$1.06^{+0.24}_{-0.23}$	$0.015^{+0.005}_{-0.003}$
1053+5200	0.04256 ± 0.00002	264.0 ± 2.0	0.204 ± 0.012	$0.27^{+0.12}_{-0.06}$	$0.97^{+0.23}_{-0.23}$	$0.068^{+0.021}_{-0.012}$
0056−0611	0.04338 ± 0.00002	376.9 ± 2.4	0.180 ± 0.010	$0.22^{+0.03}_{-0.03}$	$1.00^{+0.13}_{-0.10}$	$0.076^{+0.008}_{-0.008}$
1056+6536	0.04351 ± 0.00103	267.5 ± 7.4	0.334 ± 0.016	$0.44^{+0.18}_{-0.10}$	$1.10^{+0.23}_{-0.22}$	$0.045^{+0.014}_{-0.008}$
0923+3028	0.04495 ± 0.00049	296.0 ± 3.0	0.275 ± 0.015	$0.36^{+0.14}_{-0.09}$	$1.04^{+0.24}_{-0.22}$	$0.059^{+0.017}_{-0.011}$
1436+5010	0.04580 ± 0.00010	347.4 ± 8.9	0.234 ± 0.013	$0.30^{+0.10}_{-0.07}$	$1.02^{+0.23}_{-0.20}$	$0.071^{+0.017}_{-0.012}$
0825+1152	0.05819 ± 0.00001	319.4 ± 2.7	0.279 ± 0.021	$0.35^{+0.11}_{-0.08}$	$1.07^{+0.23}_{-0.19}$	$0.113^{+0.026}_{-0.019}$
1741+6526	0.06111 ± 0.00001	508.0 ± 4.0	0.170 ± 0.010	$0.14^{+0.00}_{-0.01}$	$1.34^{+0.07}_{-0.04}$	$0.154^{+0.004}_{-0.006}$
0755+4906	0.06302 ± 0.00213	438.0 ± 5.0	0.184 ± 0.010	$0.19^{+0.02}_{-0.03}$	$1.15^{+0.17}_{-0.10}$	$0.178^{+0.015}_{-0.019}$
2338−2052	0.07644 ± 0.00712	133.4 ± 7.5	0.258 ± 0.016	$0.34^{+0.16}_{-0.09}$	$1.01^{+0.25}_{-0.24}$	$0.261^{+0.089}_{-0.049}$
2309+2603	0.07653 ± 0.00001	405.8 ± 3.5	0.176 ± 0.010	$0.19^{+0.02}_{-0.03}$	$1.11^{+0.17}_{-0.10}$	$0.317^{+0.029}_{-0.036}$
0849+0445	0.07870 ± 0.00010	366.9 ± 4.7	0.179 ± 0.010	$0.21^{+0.04}_{-0.04}$	$1.04^{+0.19}_{-0.14}$	$0.359^{+0.049}_{-0.048}$
0751−0141	0.08001 ± 0.00279	432.6 ± 2.3	0.194 ± 0.010	$0.20^{+0.00}_{-0.00}$	$1.17^{+0.01}_{-0.01}$	$0.317^{+0.003}_{-0.004}$
2119−0018	0.08677 ± 0.00004	383.0 ± 4.0	0.159 ± 0.010	$0.19^{+0.01}_{-0.03}$	$0.99^{+0.14}_{-0.05}$	$0.530^{+0.024}_{-0.053}$
1234−0228	0.09143 ± 0.00400	94.0 ± 2.3	0.227 ± 0.014	$0.30^{+0.14}_{-0.07}$	$0.97^{+0.24}_{-0.24}$	$0.478^{+0.160}_{-0.091}$
1054−2121	0.10439 ± 0.00655	261.1 ± 7.1	0.178 ± 0.011	$0.23^{+0.09}_{-0.05}$	$0.95^{+0.23}_{-0.21}$	$0.829^{+0.217}_{-0.141}$
0745+1949	0.11240 ± 0.00833	108.7 ± 2.9	0.164 ± 0.010	$1.11^{+0.27}_{-0.77}$	$0.31^{+0.33}_{-0.03}$	$3.95^{+0.81}_{-2.41}$
1108+1512	0.12310 ± 0.00867	256.2 ± 3.7	0.179 ± 0.010	$0.23^{+0.08}_{-0.05}$	$0.96^{+0.22}_{-0.21}$	$1.27^{+0.32}_{-0.21}$
0112+1835	0.14698 ± 0.00003	295.3 ± 2.0	0.160 ± 0.010	$0.22^{+0.02}_{-0.04}$	$0.90^{+0.15}_{-0.05}$	$2.35^{+0.13}_{-0.29}$
1233+1602	0.15090 ± 0.00009	336.0 ± 4.0	0.169 ± 0.010	$0.17^{+0.02}_{-0.02}$	$1.15^{+0.16}_{-0.09}$	$1.96^{+0.15}_{-0.20}$
1130+3855	0.15652 ± 0.00001	284.0 ± 4.9	0.288 ± 0.018	$0.32^{+0.05}_{-0.06}$	$1.18^{+0.19}_{-0.12}$	$1.40^{+0.18}_{-0.19}$
1112+1117	0.17248 ± 0.00001	116.2 ± 2.8	0.176 ± 0.010	$0.23^{+0.11}_{-0.06}$	$0.93^{+0.24}_{-0.24}$	$3.25^{+1.06}_{-0.59}$
1005+3550	0.17652 ± 0.00011	143.0 ± 2.3	0.168 ± 0.010	$0.22^{+0.10}_{-0.05}$	$0.92^{+0.24}_{-0.23}$	$3.62^{+1.15}_{-0.66}$
0818+3536	0.18315 ± 0.02110	170.0 ± 5.0	0.165 ± 0.010	$0.22^{+0.10}_{-0.05}$	$0.92^{+0.24}_{-0.23}$	$4.05^{+1.26}_{-0.73}$
1443+1509	0.19053 ± 0.02402	306.7 ± 3.0	0.201 ± 0.013	$0.20^{+0.02}_{-0.03}$	$1.20^{+0.16}_{-0.09}$	$3.06^{+0.27}_{-0.31}$
1840+6423	0.19130 ± 0.00005	272.0 ± 2.0	0.182 ± 0.011	$0.21^{+0.04}_{-0.04}$	$1.04^{+0.20}_{-0.14}$	$3.76^{+0.52}_{-0.52}$
2103−0027	0.20308 ± 0.00023	281.0 ± 3.2	0.161 ± 0.010	$0.18^{+0.03}_{-0.03}$	$1.05^{+0.19}_{-0.13}$	$4.85^{+0.57}_{-0.61}$
1238+1946	0.22275 ± 0.00009	258.6 ± 2.5	0.210 ± 0.011	$0.24^{+0.04}_{-0.04}$	$1.08^{+0.19}_{-0.13}$	$4.91^{+0.62}_{-0.66}$
1249+2626	0.22906 ± 0.00112	191.6 ± 3.9	0.160 ± 0.010	$0.21^{+0.08}_{-0.05}$	$0.92^{+0.23}_{-0.22}$	$7.51^{+2.09}_{-1.31}$
0345+1748	0.23503 ± 0.00013	273.4 ± 0.5	0.218 ± 0.012	$0.27^{+0.01}_{-0.01}$	$1.02^{+0.02}_{-0.02}$	$5.80^{+0.23}_{-0.21}$
0822+2753	0.24400 ± 0.00020	271.1 ± 9.0	0.191 ± 0.012	$0.21^{+0.03}_{-0.03}$	$1.12^{+0.17}_{-0.11}$	$6.52^{+0.63}_{-0.77}$
1631+0605	0.24776 ± 0.00411	215.4 ± 3.4	0.162 ± 0.010	$0.21^{+0.07}_{-0.05}$	$0.95^{+0.22}_{-0.19}$	$8.94^{+2.05}_{-1.46}$
1526+0543	0.25039 ± 0.00001	231.9 ± 2.3	0.161 ± 0.010	$0.20^{+0.05}_{-0.04}$	$0.97^{+0.22}_{-0.17}$	$9.04^{+1.72}_{-1.41}$
2132+0754	0.25056 ± 0.00002	297.3 ± 3.0	0.187 ± 0.010	$0.17^{+0.01}_{-0.02}$	$1.26^{+0.13}_{-0.07}$	$6.43^{+0.33}_{-0.52}$
1141+3850	0.25958 ± 0.00005	265.8 ± 3.5	0.177 ± 0.010	$0.19^{+0.03}_{-0.03}$	$1.10^{+0.18}_{-0.11}$	$8.29^{+0.82}_{-0.97}$
1630+2712	0.27646 ± 0.00002	218.0 ± 5.0	0.170 ± 0.010	$0.21^{+0.06}_{-0.05}$	$0.97^{+0.22}_{-0.17}$	$11.3^{+2.2}_{-1.8}$
1449+1717	0.29075 ± 0.00001	228.5 ± 3.2	0.171 ± 0.010	$0.21^{+0.05}_{-0.04}$	$1.00^{+0.20}_{-0.15}$	$12.5^{+2.0}_{-1.8}$
0917+4638	0.31642 ± 0.00002	148.8 ± 2.0	0.173 ± 0.010	$0.23^{+0.10}_{-0.05}$	$0.94^{+0.23}_{-0.23}$	$16.5^{+5.0}_{-2.8}$
0152+0749	0.32288 ± 0.00014	217.0 ± 2.0	0.169 ± 0.010	$0.20^{+0.05}_{-0.04}$	$1.00^{+0.21}_{-0.16}$	$16.8^{+3.0}_{-2.5}$
1422+4352	0.37930 ± 0.01123	176.0 ± 6.0	0.181 ± 0.010	$0.23^{+0.08}_{-0.05}$	$0.96^{+0.22}_{-0.21}$	$25.2^{+6.4}_{-4.3}$
1617+1310	0.41124 ± 0.00086	210.1 ± 2.8	0.172 ± 0.010	$0.20^{+0.04}_{-0.04}$	$1.02^{+0.20}_{-0.14}$	$30.8^{+4.4}_{-4.3}$
1538+0252	0.41915 ± 0.00295	227.6 ± 4.9	0.168 ± 0.010	$0.18^{+0.03}_{-0.03}$	$1.09^{+0.18}_{-0.11}$	$31.4^{+3.1}_{-3.7}$
1439+1002	0.43741 ± 0.00169	174.0 ± 2.0	0.181 ± 0.010	$0.23^{+0.08}_{-0.05}$	$0.97^{+0.22}_{-0.19}$	$36.8^{+8.6}_{-6.0}$
0837+6648	0.46329 ± 0.00005	150.3 ± 3.0	0.181 ± 0.010	$0.24^{+0.09}_{-0.06}$	$0.95^{+0.23}_{-0.22}$	$43.7^{+12.0}_{-7.7}$
0940+6304	0.48438 ± 0.00001	210.4 ± 3.2	0.180 ± 0.010	$0.20^{+0.03}_{-0.03}$	$1.08^{+0.18}_{-0.12}$	$43.9^{+4.8}_{-5.4}$
0840+1527	0.52155 ± 0.00474	84.8 ± 3.1	0.192 ± 0.010	$0.25^{+0.12}_{-0.06}$	$0.95^{+0.24}_{-0.24}$	$57.5^{+18.2}_{-10.7}$
0802−0955	0.54687 ± 0.00455	176.5 ± 4.5	0.198 ± 0.012	$0.24^{+0.06}_{-0.05}$	$1.02^{+0.22}_{-0.17}$	$59.3^{+11.0}_{-9.1}$
1518+1354	0.57655 ± 0.00734	112.7 ± 4.6	0.147 ± 0.018	$0.19^{+0.09}_{-0.05}$	$0.90^{+0.26}_{-0.24}$	$97.4^{+31.0}_{-19.4}$
2151+1614	0.59152 ± 0.00008	163.3 ± 3.1	0.181 ± 0.010	$0.23^{+0.07}_{-0.05}$	$0.97^{+0.22}_{-0.18}$	$81.7^{+17.3}_{-13.3}$
1512+2615	0.59999 ± 0.02348	115.0 ± 4.0	0.250 ± 0.014	$0.33^{+0.14}_{-0.08}$	$1.01^{+0.24}_{-0.22}$	$65.1^{+19.7}_{-12.1}$
1518+0658	0.60935 ± 0.00004	172.0 ± 2.0	0.224 ± 0.013	$0.27^{+0.06}_{-0.05}$	$1.06^{+0.21}_{-0.15}$	$70.0^{+11.4}_{-10.4}$
0756+6704	0.61781 ± 0.00002	204.2 ± 1.6	0.182 ± 0.011	$0.19^{+0.02}_{-0.03}$	$1.14^{+0.17}_{-0.10}$	$79.8^{+7.1}_{-8.7}$
1151+5858	0.66902 ± 0.00070	175.7 ± 5.9	0.186 ± 0.011	$0.22^{+0.04}_{-0.04}$	$1.03^{+0.19}_{-0.14}$	105^{+15}_{-15}
0730+1703	0.69770 ± 0.05427	122.8 ± 4.3	0.182 ± 0.010	$0.24^{+0.10}_{-0.06}$	$0.94^{+0.23}_{-0.22}$	130^{+38}_{-23}

Table 3
(Continued)

Object	P (days)	k (km s^{-1})	M_1 ($M_\odot$)	M_1/M_2	$M_{\rm tot}$ ($M_\odot$)	τ (Gyr)
0308+5140	0.80590 ± 0.00109	78.9 ± 2.7	0.149 ± 0.015	$0.20^{+0.09}_{-0.05}$	$0.90^{+0.25}_{-0.24}$	233^{+75}_{-45}
0811+0225	0.82194 ± 0.00049	220.7 ± 2.5	0.179 ± 0.010	$0.14^{+0.01}_{-0.01}$	$1.45^{+0.10}_{-0.05}$	141^{+4}_{-7}
1241+0633	0.95912 ± 0.00028	138.2 ± 4.8	0.199 ± 0.012	$0.25^{+0.07}_{-0.05}$	$1.00^{+0.22}_{-0.18}$	270^{+58}_{-44}
2236+2232	1.01016 ± 0.00005	119.9 ± 2.0	0.186 ± 0.010	$0.24^{+0.09}_{-0.06}$	$0.96^{+0.23}_{-0.21}$	338^{+91}_{-58}
0815+2309	1.07357 ± 0.00018	131.7 ± 2.6	0.200 ± 0.021	$0.25^{+0.08}_{-0.06}$	$1.00^{+0.24}_{-0.19}$	367^{+85}_{-66}

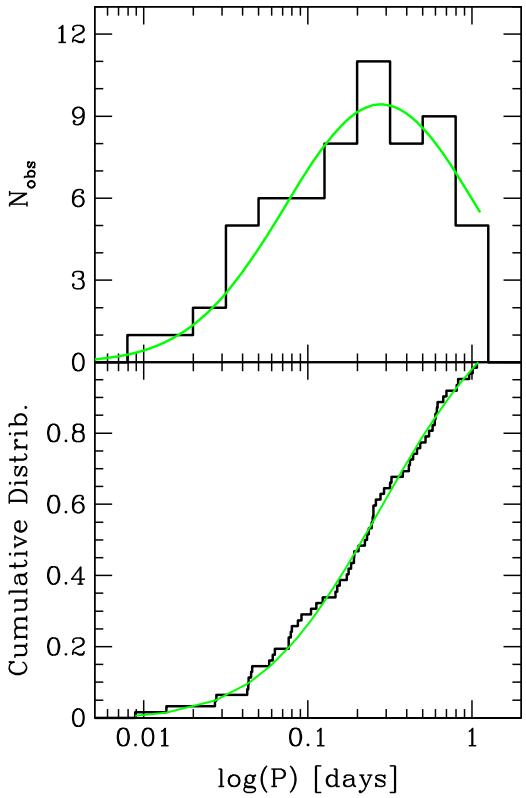

Figure 7. Observed orbital period distribution of the clean sample of 62 ELM WD binaries (black lines) compared to a lognormal fit (green lines), plotted in a histogram (upper panel) and a cumulative distribution (lower panel).

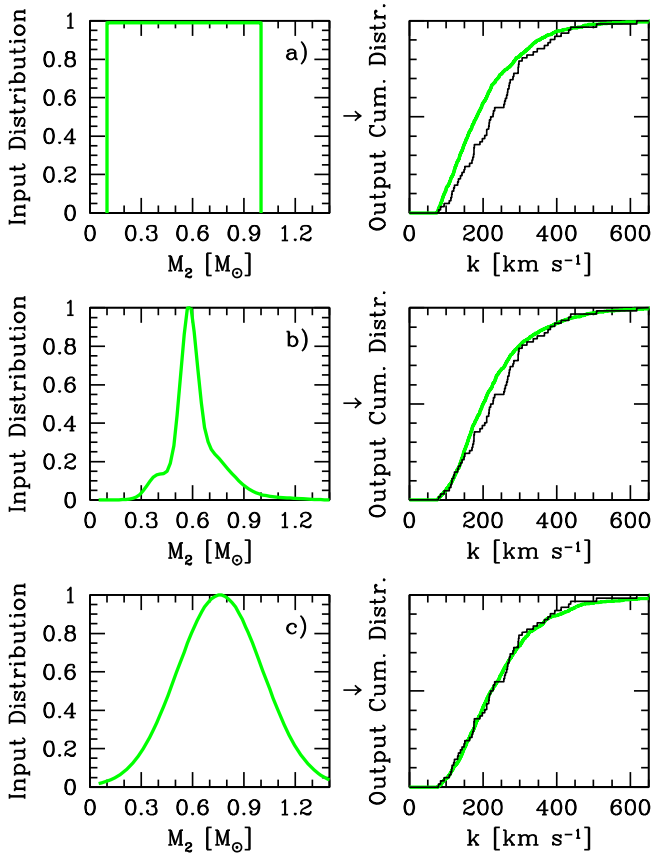

Figure 8. Trial companion mass M_2 distributions (lefthand column) and their simulated k distributions (righthand column, in green) compared with the clean sample (in black). (a) Flat M_2 distribution observed in sdB binaries, $p = 0.0012$. (b) Observed SDSS WD mass distribution, $p = 0.028$. (c) Normal M_2 distribution, $p = 0.240$.

Figure 8 presents three trial M_2 distributions and their corresponding simulated k distributions compared to the observations. At the top is the flat companion mass distribution observed in sdB binaries (Kupfer et al. 2015). The flat M_2 distribution produces a k distribution that clearly differs from the observations ($p = 0.0012$). In the middle is the WD mass distribution observed by SDSS (Kepler et al. 2007). The SDSS WD mass distribution produces a k distribution that agrees somewhat better with the observations ($p = 0.028$). Finally, we present what we find to be the best match: a normal distribution with mean $\mu_{M2} = 0.76\,M_\odot$ and standard deviation $\sigma_{M2} = 0.25\,M_\odot$. This normal distribution produces a k distribution that agrees with the clean sample of ELM WD binaries with $p = 0.240$.

Andrews et al. (2014) derive essentially the same normal distribution using an earlier version of the ELM Survey data and a different Bayesian modeling approach. Boffin (2015) also finds a similar result using an earlier version of the ELM Survey data and an inversion technique. This agreement provides us with confidence in the normal distribution result. Clearly, to fit the observed distribution of k requires a large fraction of relatively massive WD companions.

4.4. Implications

With the M_2 distribution in hand, we can go back and constrain the mass ratio, total mass, and merger time of the individual ELM WD binaries. For some of the systems we have additional constraints on inclination: two systems are eclipsing (Brown et al. 2011b; Kilic et al. 2014b), eight have ellipsoidal variations (Kilic et al. 2011c; Hermes et al. 2012a, 2014), and many more have X-ray and/or radio observations that rule out massive neutron star companions (Kilic et al. 2011a, 2012, 2014b). Combining this information with our measurements of P, k, and M_1, we calculate the distributions of M_1/M_2, $M_{\rm tot}$, and

τ for each system. The results are presented in Table 3. The columns list the median value of each distribution; the uncertainty comes from the 0.1587 and 0.8413 percentile values, equivalent to 1σ uncertainties if the quantities are normally distributed.

We find that the average total mass of the ELM WD binaries is $1.01 \pm 0.15\,M_{\odot}$. Statistically speaking, 95% of the ELM WD binaries have a total mass below the Chandrasekhar mass and thus are not type Ia supernova progenitors. This is unsurprising given the mass of the ELM WDs. However, their short orbital periods and relatively massive binary companions yield a median gravitational wave merger time of 5.8 Gyr for the sample.

The outcome of the ELM WD binary merger process depends in part on the stability of mass transfer. The ELM WD has the largest diameter of two objects in a double-degenerate binary and thus will become the donor star, the star that will fill its Roche lobe and will transfer matter to its companion when the binary evolves into contact.

A clear implication of the M_2 distribution is that the binary components have fairly extreme mass ratios, on average $M_1{:}M_2 = 1{:}3.9^{+1.2}_{-0.8}$. For this mass ratio, theorists predict that helium mass transfer rates from the donor WD should be below the rate of stable helium burning on the accretor WD (Marsh et al. 2004; Kaplan et al. 2012; Kremer et al. 2015). Thus mass transfer should proceed stably over billion year timescales, and the ELM WD binaries will become AM CVn systems (Warner 1995; Solheim 2010). However, this statement ignores an ELM WD's hydrogen envelope. If the initial hydrogen mass transfer rate is super-Eddington, a common envelope may form and cause the two WDs to quickly merge into a single massive WD (Webbink 1984; Han & Webbink 1999; Dan et al. 2011). Material ejected during shell flashes may also form a common envelope and result in a merger (Shen 2015).

Interestingly, a small peak around $1\,M_{\odot}$ is seen in the mass distribution of all WDs within 20 pc (Giammichele et al. 2012). The same peak is also seen in the mass distribution of WDs in the SDSS WD catalog (e.g., Kepler et al. 2007, 2015). Rebassa-Mansergas et al. (2015) argue that the $\simeq 1\,M_{\odot}$ peak in the WD mass distribution is more substantial than suggested in these earlier surveys. Perhaps part of the $1\,M_{\odot}$ peak in the WD mass distribution is related to the ELM WD binaries. The merger of a He+CO WD should eliminate the hydrogen atmosphere and look like an extreme helium star or R CrB star (Paczyński 1971). Whether the ELM WD binaries evolve into stable mass-transfer AM CVn systems or single massive WDs remains unclear, but it is fair to say that the binary mass ratio favors the AM CVn outcome.

5. CONCLUSION

We present 15 new ELM WD candidates, 9 of which are double degenerate binaries. This brings our targeted ELM Survey sample to 88 objects and 76 double degenerate binaries. The 12 non-variable objects in the sample are puzzling, because they exceed the number of face-on binaries we expect in a randomly oriented sample. Most of the non-variable objects have $T_{\rm eff} \simeq 8000$ K, however, and so may be related to the sdA stellar population uncovered by Kepler et al. (2016); the remaining non-variable objects would then be consistent with the number of face-on ELM WD binaries we would expect in a sample of color-selected targets.

Table 4
Radial Velocity Measurements

Object	HJD +2450000	$v_{\rm helio}$ (km s^{-1})
J0125+2017	6329.595091	30.9 ± 7.7
	6329.612901	15.8 ± 6.0
	6330.630689	41.9 ± 5.0
	6331.595507	73.8 ± 3.9
	7008.555545	0.1 ± 7.9

(This table is available in its entirety in machine-readable form.)

We show that the ELM WD binaries have a lognormal distribution of orbital period with a median period of 5.4 hr. This median period is in agreement with expectations of binary population synthesis models (Han 1998). The distribution of companion mass is best described by a normal distribution with a mean of $0.76\,M_{\odot}$. Alternative distributions, such as the observed SDSS WD mass distribution, fit the observations very poorly. The upshot is that the total mass of our ELM WD binaries is about $1\,M_{\odot}$, their mass ratio is about $M_1{:}M_2 = 1{:}4$, and their median gravitational merger time is about 6 Gyr.

An open question is the outcome of ELM WD binary mergers. Their total mass rules out type Ia supernovae. Their mass ratios argue for long-lived stable mass-transfer AM CVn binaries. Yet a merger into a single massive WD remains a possibility. Merger rates may provide a useful discriminant. Binary population synthesis models predict formation rates that differ by a factor of ten for AM CVn and R CrB stars (e.g., Zhang et al. 2014; Karakas et al. 2015). Our early ELM WD binary merger rate (Brown et al. 2011a) is a woeful underestimate given the subsequent discovery of four ELM WD binaries with <25 Myr merger times (Brown et al. 2011b; Kilic et al. 2011b, 2011c, 2014a). In the next paper, we will divide our growing and increasingly complete ELM WD binary sample into disk and halo objects, derive the space densities, and then estimate merger rates over the entire Milky Way.

We thank Charlotte Wood for her contribution to the spectral energy distributions. We thank E. Martin, A. Milone, and S. Gotilla for their assistance with observations obtained at the MMT Observatory, P. Canton for his assistance with observations obtained at Kitt Peak National Observatory, and P. Berlind and M. Calkins for their assistance with observations obtained at the Fred Lawrence Whipple Observatory. This project makes use of data products from SDSS and SDSS-II, funding for which was provided by the Alfred P. Sloan Foundation, the Participating Institutions, the National Science Foundation, the U.S. Department of Energy, the National Aeronautics and Space Administration, the Japanese Monbukagakusho, the Max Planck Society, and the Higher Education Funding Council for England. This research makes use the SAO/NASA Astrophysics Data System Bibliographic Service. This work was supported in part by the Smithsonian Institution. M.K. and A.G. gratefully acknowledge the support of the NSF and NASA under grants AST-1312678 and NNX14AF65G, respectively.

Facilities: MMT (Blue Channel Spectrograph), FLWO:1.5 m (FAST), Mayall (KOSMOS).

Table 5
Entire ELM Survey

Object	R.A. (h:m:s)	decl. (d:m:s)	$T_{\rm eff}$ (K)	$\log g$ (cm s^{-2})	Mass ($M_\odot$)	M_g (mag)	g_0 (mag)	$d_{\rm helio}$ (kpc)	P (days)	k (km s^{-1})	γ (km s^{-1})	M_2 ($M_\odot$)	τ (Gyr)
J0022+0031	0:22:28.452	0:31:15.55	20460 ± 310	7.58 ± 0.04	0.459	9.88 ± 0.08	19.284 ± 0.034	0.762 ± 0.029	0.49135 ± 0.02540	80.8 ± 1.3	−20.3 ± 0.8	>0.23	<59.25
J0022−1014	0:22:07.659	−10:14:23.53	20730 ± 340	7.28 ± 0.05	0.376	9.32 ± 0.10	19.581 ± 0.031	1.129 ± 0.052	0.07989 ± 0.00300	145.6 ± 5.6	−38.5 ± 3.7	>0.21	<0.613
J0056−0611	0:56:48.232	−6:11:41.59	12230 ± 180	6.17 ± 0.04	0.180	8.37 ± 0.10	17.208 ± 0.023	0.586 ± 0.029	0.04338 ± 0.00002	376.9 ± 2.4	4.2 ± 1.2	>0.46	<0.115
J0106−1000	1:06:57.398	−10:00:03.35	16970 ± 260	6.10 ± 0.05	0.189	7.47 ± 0.14	19.595 ± 0.023	2.669 ± 0.176	0.02715 ± 0.00002	395.2 ± 3.6	2.2 ± 2.7	>0.39	<0.036
J0112+1835	1:12:10.254	18:35:03.77	10020 ± 140	5.76 ± 0.05	0.160	8.00 ± 0.12	17.110 ± 0.016	0.664 ± 0.036	0.14698 ± 0.00003	295.3 ± 2.0	−121.4 ± 1.1	>0.62	<2.674

(This table is available in its entirety in machine-readable form.)

APPENDIX
DATA TABLES

Table 4 presents the radial velocity measurements for our 15 new ELM WD candidates. Table 4 columns include object name, heliocentric Julian date (based on UTC), and heliocentric radial velocity (uncorrected for the WD gravitational redshift).

Table 5 presents the entire ELM Survey sample of 88 objects. Table 5 columns include object name, $T_{\rm eff}$, $\log g$, estimated ELM WD mass and absolute magnitude M_g, de-reddened apparent magnitude g_0, heliocentric distance $d_{\rm helio}$, orbital period P, semi-amplitude k, systemic velocity γ, minimum secondary mass M_2, and maximum gravitational wave merger time τ.

REFERENCES

Acero, F., Ackermann, M., Ajello, M., et al. 2015, ApJS, 218, 23
Alam, S., Albareti, F. D., Allende Prieto, C., et al. 2015, ApJS, 219, 12
Althaus, L. G., Camisassa, M. E., Miller Bertolami, M. M., Córsico, A. H., & García-Berro, E. 2015, A&A, 576, A9
Althaus, L. G., Miller Bertolami, M. M., & Córsico, A. H. 2013, A&A, 557, A19
Andrews, J. J., Price-Whelan, A. M., & Agüeros, M. A. 2014, ApJL, 797, L32
Bevington, P. R., & Robinson, D. K. 1992, Data Reduction and Error Analysis for the Physical Sciences (2nd ed.; New York: McGraw-Hill)
Boffin, H. M. J. 2015, A&A, 575, L13
Bressan, A., Marigo, P., Girardi, L., et al. 2012, MNRAS, 427, 127
Brown, W. R., Beers, T. C., Wilhelm, R., et al. 2008, AJ, 135, 564
Brown, W. R., Geller, M. J., & Kenyon, S. J. 2012a, ApJ, 751, 55
Brown, W. R., Kilic, M., Allende Prieto, C., Gianninas, A., & Kenyon, S. J. 2013, ApJ, 769, 66
Brown, W. R., Kilic, M., Allende Prieto, C., & Kenyon, S. J. 2010, ApJ, 723, 1072
Brown, W. R., Kilic, M., Allende Prieto, C., & Kenyon, S. J. 2011a, MNRAS, 411, L31
Brown, W. R., Kilic, M., Allende Prieto, C., & Kenyon, S. J. 2012b, ApJ, 744, 142
Brown, W. R., Kilic, M., Hermes, J. J., et al. 2011b, ApJL, 737, L23
Dan, M., Rosswog, S., Guillochon, J., & Ramirez-Ruiz, E. 2011, ApJ, 737, 89
Eisenstein, D. J., Liebert, J., Harris, H. C., et al. 2006, ApJS, 167, 40
Fabricant, D., Cheimets, P., Caldwell, N., & Geary, J. 1998, PASP, 110, 79
Geller, A. M., Latham, D. W., & Mathieu, R. D. 2015, AJ, 150, 97
Geller, A. M., & Mathieu, R. D. 2012, AJ, 144, 54
Giammichele, N., Bergeron, P., & Dufour, P. 2012, ApJS, 199, 29
Gianninas, A., Bergeron, P., & Ruiz, M. T. 2011, ApJ, 743, 138
Gianninas, A., Dufour, P., Kilic, M., et al. 2014, ApJ, 794, 35
Gianninas, A., Kilic, M., Brown, W. R., Canton, P., & Kenyon, S. J. 2015, ApJ, 812, 167
Hallakoun, N., Maoz, D., Kilic, M., et al. 2016, MNRAS, submitted
Han, Z. 1998, MNRAS, 296, 1019
Han, Z., & Webbink, R. F. 1999, A&A, 349, L17
Heber, U. 2009, ARA&A, 47, 211
Heber, U., Edelmann, H., Lisker, T., & Napiwotzki, R. 2003, A&A, 411, L477
Hermes, J. J., Brown, W. R., Kilic, M., et al. 2014, ApJ, 792, 39
Hermes, J. J., Kilic, M., Brown, W. R., Montgomery, M. H., & Winget, D. E. 2012a, ApJ, 749, 42
Hermes, J. J., Kilic, M., Brown, W. R., et al. 2012b, ApJL, 757, L21
Hermes, J. J., Montgomery, M. H., Gianninas, A., et al. 2013a, MNRAS, 436, 3573
Hermes, J. J., Montgomery, M. H., Winget, D. E., et al. 2012c, ApJL, 750, L28
Hermes, J. J., Montgomery, M. H., Winget, D. E., et al. 2013b, ApJ, 765, 102
Iben, I., Jr. 1990, ApJ, 353, 215
Istrate, A. G., Tauris, T. M., Langer, N., & Antoniadis, J. 2014, A&A, 571, L3
Kaplan, D. L., Bhalerao, V. B., van Kerkwijk, M. H., et al. 2013, ApJ, 765, 158
Kaplan, D. L., Bildsten, L., & Steinfadt, J. D. R. 2012, ApJ, 758, 64
Karakas, A. I., Ruiter, A. J., & Hampel, M. 2015, ApJ, 809, 184
Kenyon, S. J., & Garcia, M. R. 1986, AJ, 91, 125
Kepler, S. O., Kleinman, S. J., Nitta, A., et al. 2007, MNRAS, 375, 1315
Kepler, S. O., Pelisoli, I., Koester, D., et al. 2015, MNRAS, 446, 4078
Kepler, S. O., Pelisoli, I., Koester, D., et al. 2016, MNRAS, 455, 3414
Kilic, M., Brown, W. R., Allende Prieto, C., Kenyon, S. J., & Panei, J. A. 2010, ApJ, 716, 122
Kilic, M., Brown, W. R., Allende Prieto, C., et al. 2011a, ApJ, 727, 3
Kilic, M., Brown, W. R., Allende Prieto, C., et al. 2012, ApJ, 751, 141
Kilic, M., Brown, W. R., Gianninas, A., et al. 2014a, MNRAS, 444, L1
Kilic, M., Brown, W. R., Hermes, J. J., & Gianninas, A. 2015a, ApSSP, 40, 167
Kilic, M., Brown, W. R., Hermes, J. J., et al. 2011b, MNRAS, 418, L157
Kilic, M., Brown, W. R., Kenyon, S. J., et al. 2011c, MNRAS, 413, L101
Kilic, M., Hermes, J. J., Gianninas, A., & Brown, W. R. 2015b, MNRAS, 446, L26
Kilic, M., Hermes, J. J., Gianninas, A., et al. 2014b, MNRAS, 438, L26
Kleinman, S. J., Kepler, S. O., Koester, D., et al. 2013, ApJS, 204, 5
Kraft, R. P., Mathews, J., & Greenstein, J. L. 1962, ApJ, 136, 312
Kremer, K., Sepinsky, J., & Kalogera, V. 2015, ApJ, 806, 76
Kupfer, T., Geier, S., Heber, U., et al. 2015, A&A, 576, A44
Kurtz, M. J., & Mink, D. J. 1998, PASP, 110, 934
Lawrence, A., Warren, S. J., Almaini, O., et al. 2007, MNRAS, 379, 1599
Marsh, T. R., Dhillon, V. S., & Duck, S. R. 1995, MNRAS, 275, 828
Marsh, T. R., Nelemans, G., & Steeghs, D. 2004, MNRAS, 350, 113
Martin, D. C., Fanson, J., Schiminovich, D., et al. 2005, ApJL, 619, L1
Martini, P., Elias, J., Points, S., et al. 2014, Proc. SPIE, 9147, 91470Z
Massey, P., Strobel, K., Barnes, J. V., & Anderson, E. 1988, ApJ, 328, 315
Maxted, P. F. L., Marsh, T. R., & Moran, C. K. J. 2000, MNRAS, 319, 305
Moran, C., Marsh, T. R., & Bragaglia, A. 1997, MNRAS, 288, 538
Nebot Gómez-Morán, A., Gänsicke, B. T., Schreiber, M. R., et al. 2011, A&A, 536, A43
Paczyński, B. 1971, AcA, 21, 1
Panei, J. A., Althaus, L. G., Chen, X., & Han, Z. 2007, MNRAS, 382, 779
Parsons, S. G., Marsh, T. R., Gänsicke, B. T., Drake, A. J., & Koester, D. 2011, ApJL, 735, L30
Press, W. H., Teukolsky, S. A., Vetterling, W. T., & Flannery, B. P. 1992, Numerical Recipes in C, The Art of Scientific Computing (2nd ed.; Cambridge: Cambridge Univ. Press)
Rebassa-Mansergas, A., Gänsicke, B. T., Schreiber, M. R., Koester, D., & Rodríguez-Gil, P. 2010, MNRAS, 402, 620
Rebassa-Mansergas, A., Nebot Gómez-Morán, A., Schreiber, M. R., et al. 2012, MNRAS, 419, 806
Rebassa-Mansergas, A., Rybicka, M., Liu, X.-W., Han, Z., & García-Berro, E. 2015, MNRAS, 452, 1637
Sarna, M. J., Ergma, E., & Gerškevitš-Antipova, J. 2000, MNRAS, 316, 84
Schmidt, G. D., Weymann, R. J., & Foltz, C. B. 1989, PASP, 101, 713
Scholz, F. W., & Stephens, M. A. 1987, J. Am. Stat. Assoc., 82, 918
Schreiber, M. R., Gänsicke, B. T., Rebassa-Mansergas, A., et al. 2010, A&A, 513, L7
Shen, K. J. 2015, ApJL, 805, L6
Silvotti, R., Østensen, R. H., Bloemen, S., et al. 2012, MNRAS, 424, 1752
Skrutskie, M. F., Cutri, R. M., Stiening, R., et al. 2006, AJ, 131, 1163
Solheim, J. 2010, PASP, 122, 1133
Steinfadt, J. D. R., Kaplan, D. L., Shporer, A., Bildsten, L., & Howell, S. B. 2010, ApJL, 716, L146
Tremblay, P.-E., & Bergeron, P. 2009, ApJ, 696, 1755
Tremblay, P.-E., Gianninas, A., Kilic, M., et al. 2015, ApJ, 809, 148
Tremblay, P.-E., Ludwig, H.-G., Steffen, M., & Freytag, B. 2013, A&A, 559, A104
Vennes, S., Thorstensen, J. R., Kawka, A., et al. 2011, ApJL, 737, L16
Warner, B. 1995, Ap&SS, 225, 249
Webbink, R. F. 1984, ApJ, 277, 355
Wright, E. L., Eisenhardt, P. R. M., Mainzer, A. K., et al. 2010, AJ, 140, 1868
Zhang, X., Jeffery, C. S., Chen, X., & Han, Z. 2014, MNRAS, 445, 660